Shahrood University of Technology
Iranian Society of Mining Engineering (IRSME)

Journal of Mining and Environment (JME)

journal homepage: www.jme.shahroodut.ac.ir

THOMSON REUTERS

Vol. 11, No. 3, 2020, 675-693.
DOI: 10.22044/jme.2020.9045.1793

Investigation of Effect of Number of Lifters on Performance of Pilot-Scale SAG Mills Using Discrete Element Method

S. Kolahi and M. Jahani Chegeni*

Faculty of Mining, Petroleum & Geophysics Engineering, Shahrood University of Technology, Shahrood, Iran

Received 21 October 2020; received in revised form 7 February 2020; accepted 14 February 2020

Keywords

DEM simulation

Pilot-scale SAG Mill

Number of Lifters

Head height

Impact zone length

Abstract

The number of lifters of mill shell liners, mill rotation speed, and filling percentage of grinding media are three of the most important parameters influencing the charge behavior and the trajectory of ball motion inside the SAG mills, and consequently, their performance. In this paper, the milling operation of pilot-scale SAG mills using the discrete element method (DEM) is investigated. First, a pilot-scale SAG mill with dimensions of 3.0 m × 1.5 m with no lifter is simulated. Then by adding, respectively, one, two, four, eight, sixteen, and thirty-two rectangle lifter(s), six other independent simulations are performed. The effects of the number of lifters on the two new parameters introduced by the authors, i.e. 'head height' and 'impact zone length' as well as on creation of cascading, cataracting, and centrifuging motions for balls at two different mill speeds, i.e. 70% and 80% of its critical speed (NC), are evaluated. Also in order to validate the simulation results, a laboratory-scale SAG mill is simulated. The results obtained indicate that the optimum number of lifters for pilot-scale SAG mills is between 16 and 32 lifters with medium thickness. Liners with the number of lifters in this range require less mill speed to create cataract motions. However, liners with the number of lifters less than this range require a higher mill speed. Also liners with the number of lifters beyond this range require less mill speed, and can cause centrifugal motions in the balls. Comparison of the simulations related to the laboratory-scale SAG mill with experimental results demonstrates a good agreement, which validates the DEM simulations and the software used.

1. Introduction

Grinding is the most common process used to liberate the valuable minerals from the gangue. Tumbling mills have been used mainly in the mineral processing industry since the mid-19th century due to the need for a finer material. However, there is still a need for understanding the combined and individual effects of all design and operating variables to make the process more efficient [1]. Mishra and Rajamani [2] were the first ones to track the motion of the ball charge in large-diameter ball mills using discrete element method (DEM) simulation. Later, Powell and McBride [3] illustrated the media motion and grinding regions (head, departure shoulder, circulation center, equilibrium surface, bulk toe, and impact toe). In the past three decades, the importance of lifter on the charge behavior in tumbling mills has been discussed. Cleary [4, 5] has used DEM to predict the wear of lifters and the power draw of SAG mills. Kalala et al. [6, 7] have investigated the wear of lifter profiles for the mills grinding dry coal. Banisi and Hadizadeh [8] have used a mechanical lifter wear monitor to measure the mass loss due to the wear in SAG mill. Modification of SAG mill liner shape based on 3D liner wear profile measurements has been conducted by Yahyaei et al. [9]. Many researchers have been working on simulating the SAG mills

Corresponding author: m.jahani1983@gmail.com (M. Jahani Chegeni).

using the DEM method [10–23]. Examples of 3D models of SAG mills have been presented along with detailed predictions of power draw, liner wear rates, liner stresses, and energy spectra by Cleary [10]. Abd El-Rahman et al. have indicated that DEM successfully predicts power draft in a variety of SAG plant operations [11]. Predictions of flow patterns in a 600-mm scale model SAG mill has been made using four classes of DEM models and have been compared to experimental photographs by Cleary et al. [12]. A review of computer simulation of tumbling mills by DEM has been conducted by Mishra [13], where practical applications of DEM have been studied. Various ways of extracting collision data from the DEM model and translating it into breakage estimates have been described by Morrison and Cleary [14], where the different breakage mechanisms (impact and abrasion) and the specific impact histories of the particles in order to assess the breakage rates for various size fractions in the mills have been investigated. DEM has been used by Djordjevic et al. [15] to model the effects of lifter height (5–25cm) and mill speed (50–90% of critical) on the power draw and frequency distribution of specific energy (J/kg) of normal impacts in a 5 m diameter autogenous (AG) mill. Also comminution patterns within a pilot scale AG/SAG mill have been modeled by Djordjevic et al. [16]. By gradually increasing the tumbling model SAG mill length and analyzing the charge trajectory and shape variation at given operating conditions (i.e. ball filling, mill speed, liner type), the impact of end-wall effect on the charge trajectory in model mills has been investigated by Maleki-Moghaddam et al. [17]. A relationship between charge shape characteristics and fill level and lifter height for a SAG mill has been obtained by Owen and Cleary [18]. Estimating energy in grinding using DEM modeling has been conducted by Weerasekara et al. [19], where they have explored the breakage environment in mills using DEM techniques, and how these techniques may be expanded to provide more useful data for mill and comminution device modeling. A campaign of DEM simulations has been performed by varying the mill size and charge particle size distribution to explore and understand the breakage environment in mills using the DEM techniques [19]. Analysis of each mill has been conducted through consideration of the total energy dissipation and the nature of the collision environment that leads to comminution [19]. Development of models relating charge shape and power draw to SAG mill operating parameters and their use in devising mill operating strategies to account for liner wear has been conducted by Cleary and Owen [20]. Numerical prediction of wear in SAG mills based on DEM simulations has been performed by Xu et al. [21], where the 3D simulations have been performed using DEM combined with an erosion model, which is referred to as Shear Impact Energy Model (SIEM), to predict wear within a SAG mill. Effect of operating condition changes on the collisional environment in a SAG mill has been investigated by Cleary and Owen [22]. The role of end liners in dry SAG mills with the objective of obtaining a thorough understanding of the effects of end liners design on the load trajectory and SAG mill performance has been experimentally studied by Hasankhoei et al. [23]. The test works have been conducted in a scale down mill with a diameter of 1 m. It was shown that the liner in the first and the last 20% of the mill length which were under the protection of the deflector liners experienced no deformation [23].

Grinding consumes most of the energy in mineral processing. SAG mill is an important kind of grinding equipment used to decrease the size of ore particles. The power consumption of a SAG mill is one of the most important parameters to consider in the design of a SAG mill because it determines its economic efficiency. The power consumption is usually determined by charge fill level, lifter height, lifter number, and mill speed. However, almost all the classical theories for calculating the power consumption of SAG mills disregard the effect of lifters, and only focus on rotation rate and charge fill level, as well as size and shape of grinding media, and thereby may cause errors [24]. Mill liners protect mill shells from abrasion and lift ore particles and grinding media to a high position. Therefore, liners/lifters must be able to bear high-impact loads during the grinding process. The wear rate of these components is high, and these parts tend to break or incur wear-out failure, which can seriously affect the production efficiency of SAG mills. Thus the research works on liner structure and configuration of SAG mills is crucial to improve the production ability and economy of SAG mills [24].

The mineral processing industry could save about 70% of the power involved in grinding processes if this power is reduced to its practical minimum power consumption [25]. In this context, achieving a more efficient grinding in SAG mills is an important issue since they have a low efficiency rate partially due to lack of creation of cascading and cataracting motions for balls and inappropriate shoulder and toe points [26]. For a given number of balls, if the mill rotation speed is higher than or

equal to its critical speed, the balls stick to the mill wall and the grinding operation does not occur and centrifuging motions are created. On the other hand, if the mill speed is between 80% and 100% of its critical speed, the suitable shoulder and toe points are not created and the grinding energy is used to hit the balls with the mill wall; in this mode, centrifuging motions are also created. However, if the mill speed is between 60% and 80% of its critical speed, the appropriate shoulder and toe points as well as the cascading and cataracting motions are created, which result in a better grinding. In this case, the dominant mechanism will be impact, which is the optimum mode for the process and will reduce the power consumption of the mill. Meanwhile, the abrasion mechanism is not very effective in this mode. At speeds less than 60% of the critical speed, the cascading and cataracting motions gradually disappear and the balls roll over each other. In this case, grinding is not optimal and the abrasion mechanism plays a more effective role [26]. Among other effective factors on creating the cascading and cataracting motions in mills, lifters can be mentioned. Lifters cause the balls to climb to a higher elevation and prevent their slipping [26].

Simulation has become a common tool in the design and optimization of industrial processes [27–29]. The continuous increase in computing power is now enabling the researchers to implement the numerical methods that do not focus on the granular assembly as an entity but rather deduce its global characteristics from observing the individual behavior of each particle [30]. Due to their discontinuous nature, one should expect that granular media require a discontinuous simulation method. Indeed, to date, DEM is the leading approach to those problems [30]. Because of its inherent advantages in analyzing granular materials, DEM has been developed rapidly in the recent decades and is used widely in mineral processing engineering [31–33].

In order to control, optimize, and reduce SAG mill power consumption, mineral processing engineers have to obtain enough information about their operation conditions. One of the most effective techniques is the use of computer simulations. Computer simulations using methods such as DEM can be effective to find optimal speed of SAG mills, and as a result, creating appropriate shoulder and toe points in them as well as creating the cascading and cataracting motions. This method can also be used to prevent centrifugal motions. In this research, DEM is introduced and used, utilizing an open-source software, LIGGGHTS, to simulate milling operation of the pilot-scale SAG mills. A pilot-scale SAG mill with no lifter was simulated by this method. Then by adding, respectively, one, two, four, eight, sixteen, and thirty-two rectangle lifter(s), six other independent simulations are performed. Also, in this paper, it has been shown that ‘shoulder height’ and ‘toe height’, which are used in all previous investigations by the researchers to evaluate and determine the trajectory of ball motion, are not suitable criteria for investigating the impact mechanism and improving the mill performance. For this reason, for the first time, two new parameters, called ‘head height’ and ‘impact zone length’, are introduced by the authors instead of them. The charge ‘head height’ means the highest altitude when the particles begin to detach from the mill and begin their cataracting motion. Also the ‘impact zone length’ is the difference in the length of the toe point with the highest end point of the cataract motion (impact point) (Figure 1). Additionally, the effects of mill shell liner type on the charge shoulder, toe, impact, and head points, also on head height and impact zone length as well as on creation of cascading, cataracting, and centrifuging motions for balls at two different mill speeds, i.e. 70% and 80% of its critical speed (CS) are evaluated. Also in order to validate the simulation results, a laboratory-scale SAG mill is simulated. In summary, in this research, for the first time, the effect of the number of lifters on two new parameters introduced by the authors, i.e. ‘head height’ and ‘impact zone length’, and as a result, on the impact mechanism and performance of pilot-scale SAG mills at different mill speeds (70% and 80% of CS) using discrete element method were investigated. The main innovation and novelty of this paper are introducing and basing ‘head height’ and ‘impact zone length’ to evaluate and determine the trajectory of ball motion for investigating the impact mechanism and improving the mill performance.

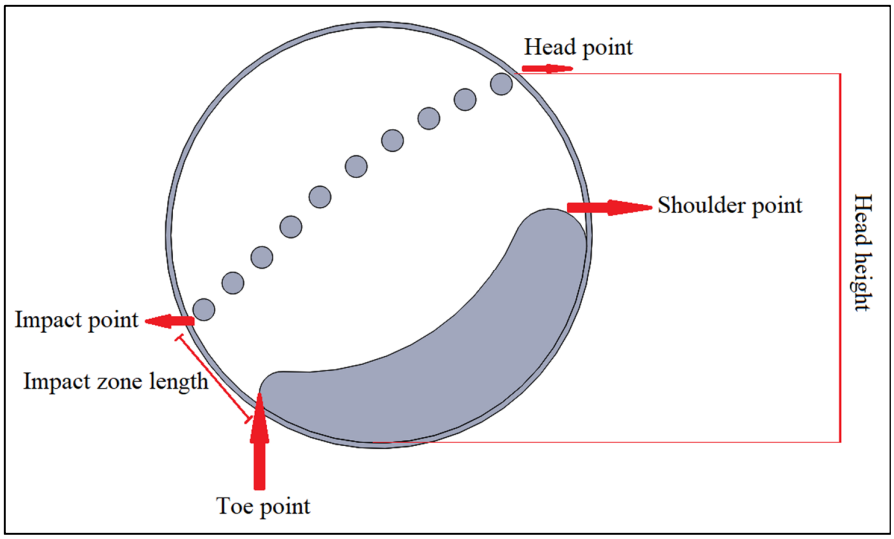

Figure 1. Charge head, shoulder, toe, and impact points as well as head height and impact zone length.

2. Simulation method

2.1. DEM to predict particle flow

DEM is a numerical technique used to predict the behavior of collision dominated particle flows. Each particle in the flow is tracked and all collisions between particles and between particles and boundaries are modeled. DEM is a powerful numerical tool for simulating the mechanical behavior of the systems with a large number of particles based on the particles' motion and interactions and their representation as rigid geometric bodies, commonly having a spherical shape [34, 35], whereas simulations with spherical particles can include millions of particles using non-spherical particles is still not an easy task. For spherical particles, the geometry is described by the radius and the interaction forces that can easily be calculated by the contact laws like Hertzian contact, for non-spherical particles, the geometry representation and calculation of contact forces are much more complex [34, 36]. DEM is based on the Lagrangian approach and treats granular material as an assemblage of distinct particles, each governed by physical laws [37, 38]. Each particle interacts with its neighbors through particle-to-particle contacts, which can be formed or broken at each time step [35, 37, 39–41]. In the recent years, the drastic increase in affordable computational power has allowed the DEM simulations to become a versatile tool for industrial applications [42]. The recent advances in discrete element modeling have resulted in this method becoming a useful simulation tool that can provide detailed information not easily measured during experiments [43]. With the maturing of DEM simulation, it has now become possible to run simulations of millions of particles with complex shapes and inter-particle cohesive forces in tolerable times on single processor, desktop computers [27, 42–44].

In this research, an open-source software, LIGGGHTS, was used to perform the DEM simulations. The DEM variant used here is sometimes called a 'soft particle method'. The particles are allowed to overlap, and the extent of overlap is used in conjunction with a contact force law to give instantaneous forces from knowledge of the current positions, orientations, velocities and spins of the particles [45]. Here, we have used the Hertz–Mindlin's contact force law. It states that the repulsive force resulting from a collision is calculated from the amount of normal overlap δ_n and tangential overlap δ_t (soft-sphere approach) [46]. This granular model uses the following formula for the frictional force between two granular particles, when the distance r between two particles of radii R_i and R_j is less than their contact distance $d = R_i + R_j$. There is no force between the particles when $r > d$:

$$\mathbf{F} = \left(k_n \boldsymbol{\delta n}_{ij} - \gamma_n \mathbf{v n}_{ij}\right) + \left(k_t \boldsymbol{\delta t}_{ij} - \gamma_t \mathbf{v t}_{ij}\right) \qquad (1)$$

The first term is the normal force ($\mathbf{F_n}$) between the two particles and the second term is the tangential force ($\mathbf{F_t}$). The normal force has two terms: a spring force and a damping force. The tangential force also has two terms: a shear force and a damping force. The shear force is a "history" effect that accounts for the tangential displacement (tangential overlap) between the particles for the duration of the time they are in contact.

The quantities in the equation are as follow:

k_n: elastic constant for normal contact;
$\boldsymbol{\delta n_{ij}}$: d − r = normal overlap (overlap distance between the two particles);
γ_n: viscoelastic damping constant for normal contact;
$\mathbf{vn_{ij}}$: normal relative velocity (normal component of the relative velocity of the two particles);
k_t: elastic constant for tangential contact;
$\boldsymbol{\delta t_{ij}}$: tangential overlap (tangential displacement vector between the two spherical particles, which is truncated to satisfy a frictional yield criterion);
γ_t: viscoelastic damping constant for tangential contact;
$\mathbf{vt_{ij}}$: tangential relative velocity (tangential component of the relative velocity of the two particles).

Considering that the shear modulus (G) can be calculated from Young's modulus and Poisson ratio, the Hertz–Mindlin contact model depends on the following material parameters [46]:

Coefficient of restitution, e;
Young's modulus, Y;
Poisson ratio, ν;
Coefficient of static friction, μ_s;
Coefficient of rolling friction, μ_r.

The maximum overlap between particles is determined by the stiffness k_n of the spring in the normal direction. Typically, average overlaps of 0.1–0.5% are desirable, requiring spring constants of the order of 10^4–10^6 N/m in three dimensions. The normal damping coefficient γ_n is chosen to give the required coefficient of restitution e (defined as the ratio of the post-collisional to pre-collisional normal component of the relative velocity) [47].

In DEM, the particles are traditionally approximated by disks or spheres, in two and three dimensions, respectively. These shapes are preferred because of their computational efficiency. The contact is always on the line joining the center of each particle and is as simple as comparing the distance between their centers to the sum of their radii [42, 44]. Since in a SAG mills, balls are spherical, DEM can be appropriately used to simulate their motion.

The drawback of the DEM method is that the time step has to be chosen extremely small because the contact force exhibits a very stiff behavior. Depending on the material properties and the particle size the time step size can be as low as 10^{-6} s for an accurate simulation [48–50].

3. SAG mill configuration

In this work, a pilot-scale SAG mill with no lifter was simulated by DEM. Then by adding, respectively, one, two, four, eight, sixteen, and thirty-two rectangle lifter(s), six other independent simulations were performed (Figure 2). It is worth noting that the addition of 64 lifters to the mill would greatly increase the kinetic energy of the particles and tear the geometry. Also adding more lifters to the mill made the mill look like a smooth mode (no-lifter case) .Therefore, it is not possible to add more lifters.

The detailed geometrical and operational conditions and material properties and calculations for these pilot-scale SAG mills are listed in Tables 1–4. It should be noted that the material of the SAG balls used in the simulations are stainless steel.

Table 1. Pilot-scale SAG mill dimensions and speeds.

Pilot-scale SAG mill	Dimensions
Shell thickness (cm)	12.5
Mill length (m)	1.5
Mill diameter (m)	3.0
Mill volume (m^3)	10.6029
N_C (critical speed) (rpm)	24.67
Rotation speed (70% of N_C) (rpm)	17.27
Rotation speed (80% of N_C) (rpm)	19.74
Direction of rotation of mill	**Counter-clockwise**
Rectangle lifter length (m)	1.5
Rectangle lifter height (cm)	12.5
Rectangle lifter width (cm)	12.5

Table 2. DEM ball size distribution and specification.

Ball size class (mm)	Mass fraction (%)
60	100

Table 3. DEM ball specifications and calculations.

Ball diameter (mm)	60
Ball radius (mm)	30
Volume of one ball (m^3)	1.1310×10^{-4}
Volume of all balls (m^3)	$7.5\% \times 10.6029 = 0.7952$
# Balls	$0.7952/1.1310 \times 10^{-4} = 7032$
Total mass of balls (kg)	$8050 \times 0.7952 = 6401.49$
Mass rate (kg)	640.15 (10 steps)
Period of 70% N_C	60/17.27 = 3.4745
Period of 80% N_C	60/19.74 = 3.0401
Neighbor (particle interaction distance) (m)	$5\% \times 30$ mm $= 15 \times 10^{-4}$

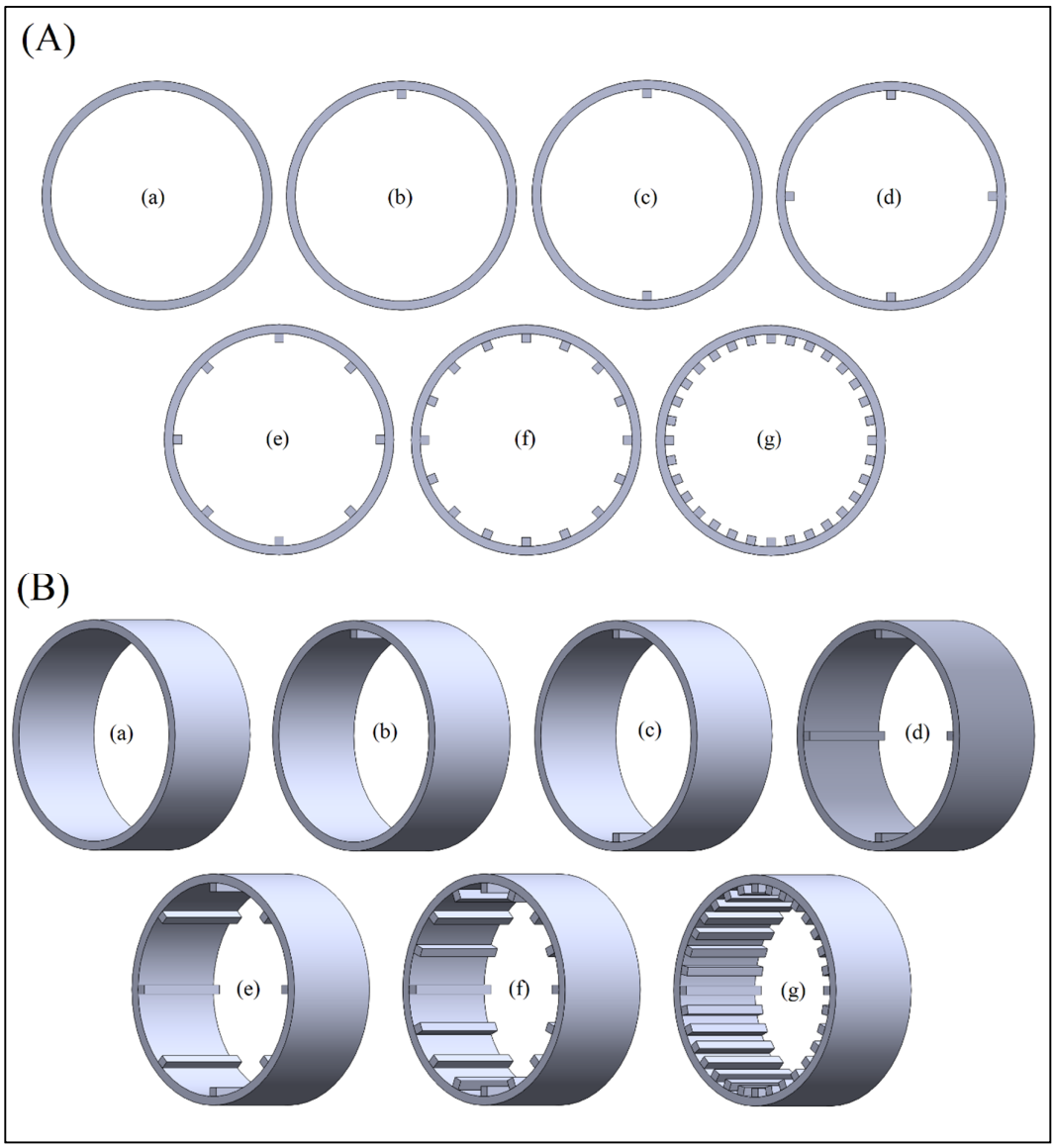

Figure 2. 2D (A) and 3D (B) geometries of pilot-scale SAG mills with (a) no lifter; (b) one rectangle lifter; (c) two rectangle lifters; (d) four rectangle lifters; (e) eight rectangle lifters; (f) sixteen rectangle lifters; (g) thirty-two rectangle lifters.

Table 4. Parameters used for DEM simulations of the pilot-scale SAG mill.

DEM model details	Value
% Fill of ball charge	15
# DEM balls in simulation	7030
Total mass of ball charge (kg)	6401.49
DEM spring constant (kg/m)	10^6
Ball density (kg/m^3)	8050
Ball sliding friction coefficient	0.5
Ball rolling friction coefficient	0.0015
Poisons ratio	0.285
Young's modulus (N/m^2)	1×10^9
Ball restitution coefficient	0.817

4. Results and discussion

Figure 3 demonstrates snapshots of 2D and 3D of the simulations of the pilot-scale SAG mill with no lifter, one lifter, two lifters, four lifters, eight lifters, sixteen lifters, and thirty-two lifters when the drum was rotating at 70% of its critical speed using DEM, respectively. Also Figure 4 demonstrates snapshots of 2D and 3D of the simulations of the pilot-scale SAG mill with no lifter, one lifter, two lifters, four lifters, eight lifters, sixteen lifters, and thirty-two lifters when the drum was rotating at 80% of its critical speed using DEM, respectively.

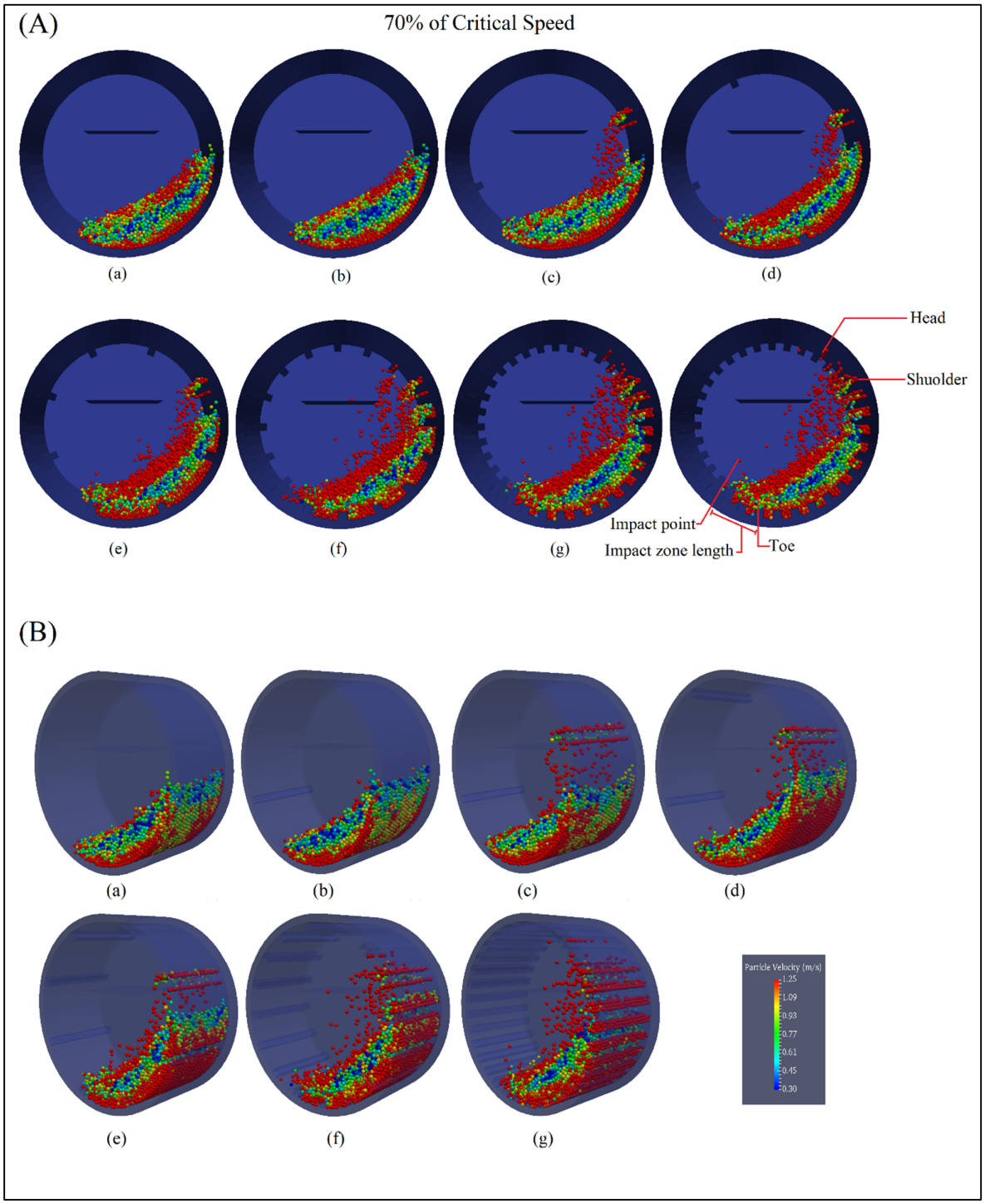

Figure 3. 2D (A) and 3D (B) snapshots showing the motion of particles on the pilot-scale SAG mill with (a) no lifter; (b) one lifter; (c) two lifters; (d) four lifters; (e) eight lifters; (f) sixteen lifters; (g) thirty-two lifters (head, shoulder, toe, and impact points as well as impact zone length are marked on the Figure) when the drum was rotating at 70% of its critical speed using DEM.

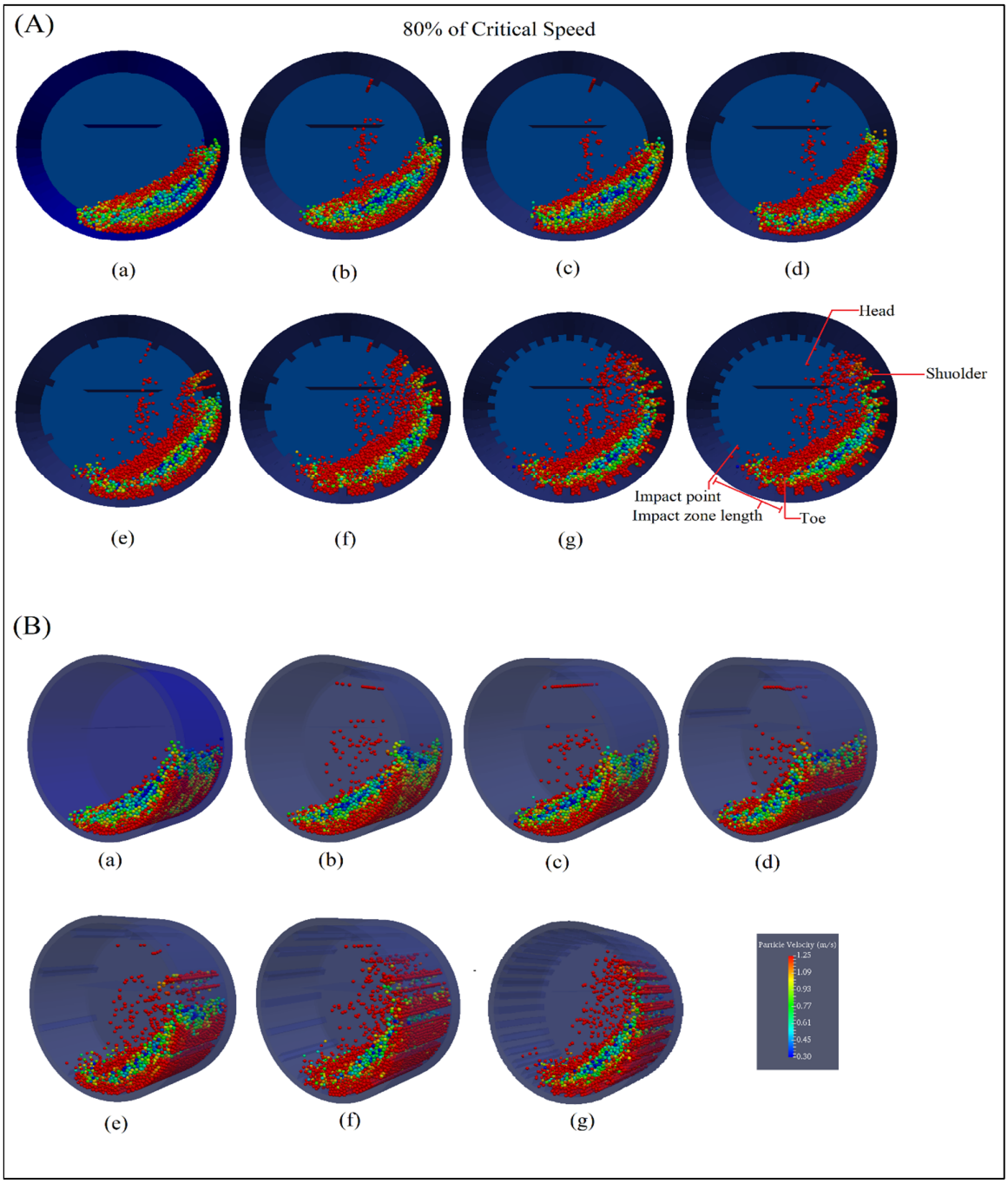

Figure 4. 2D (A) and 3D (B) snapshots showing the motion of particles on the pilot-scale SAG mill with (a) no lifter; (b) one lifter; (c) two lifters; (d) four lifters; (e) eight lifters; (f) sixteen lifters; (g) thirty-two lifters (head, shoulder, toe, and impact points as well as impact zone length are marked on the Figure) when the drum was rotating at 80% of its critical speed using DEM.

Figure 5 demonstrates how to measure the angle of the charge shoulder, toe, and head points (degree) as well as the impact zone length (cm) using an online protractor in the pilot-scale SAG mill with no lifter, one lifter, two lifters, four lifters, eight lifters, sixteen lifters, and thirty-two lifters, respectively, when the drum was rotating at 70% and 80% of its critical speed using DEM.

The exact values of the height (cm) and the angle of the charge shoulder, toe, and head points of the balls are available for no-lifter, one lifter, two lifters, four lifters, eight lifters, sixteen lifters, and thirty-two lifters mills in Table 5.

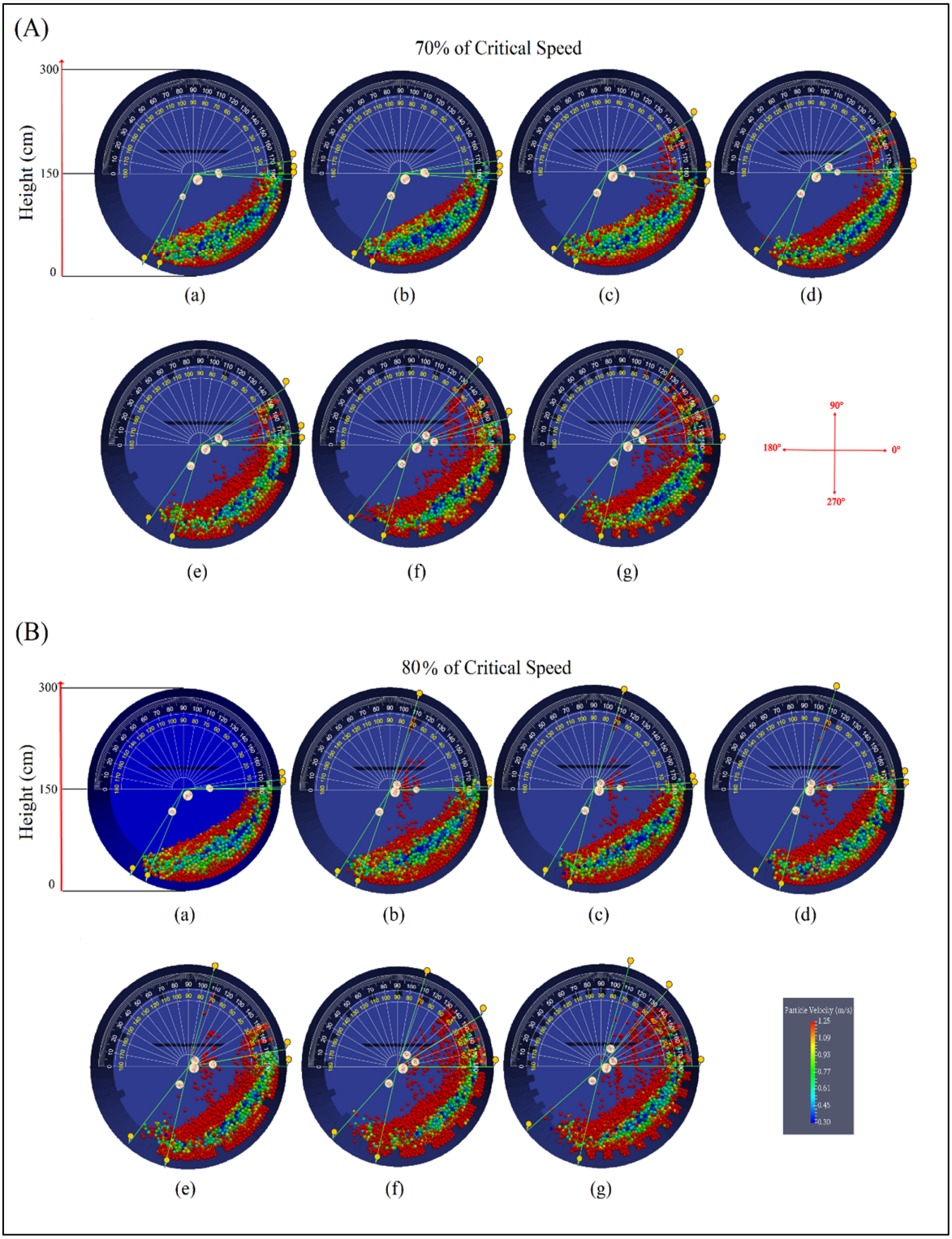

Figure 5. Using an online protractor to determine the height (cm) and angle (degree) of the shoulder, toe, and head points as well as impact zone length (cm) in the pilot-scale SAG mill with (a) no lifter; (b) one lifter; (c) two lifters; (d) four lifters; (e) eight lifters; (f) sixteen lifters; (g) thirty-two lifters when the drum was rotating at 70% (A) and 80% (B) of its critical speed using DEM.

Table 5 - Values of the height and angle of the shoulder, toe, and head points as well as impact zone length of the balls for no-lifter, one lifter, two lifters, four lifters, eight lifters, sixteen lifters, and thirty-two lifters pilot-scale SAG mills.

Mill type	Critical speed (%)	Cascade motion	Cataract motion	Centrifuge motion	Toe height (cm)	Shoulder height (cm)	Head height (cm)	Impact zone length (cm)	Toe angle (degree)	Shoulder angle (degree)	Head angle (degree)	Impact zone angle (degree)
No-lifter mill	70	yes	no	no	7.34	142.15	168.28	23.54	252	-3	7	243
1-lifter mill	70	yes	no	no	7.34	139.54	168.28	31.36	252	-4	7	240
2-lifters mill	70	yes	yes	no	9.05	126.53	227.26	39.16	250	-9	31	235
4-lifters mill	70	yes	yes	no	9.05	155.23	227.26	41.75	250	2	31	234
8-lifters mill	70	yes	yes	no	6.55	168.28	231.70	44.34	253	7	33	236
16-lifters mill	70	yes	yes	no	7.34	186.29	261.47	57.24	252	14	48	230
32-lifters mill	70	yes	yes	no	3.84	227.26	274.36	64.93	257	31	56	232
No-lifter mill	80	yes	no	no	9.96	152.62	163.07	26.15	249	1	5	239
1-lifter mill	80	yes	yes	no	7.34	155.23	292.66	33.96	252	2	72	239
2-lifters mill	80	yes	yes	no	9.96	157.85	292.66	41.75	249	3	72	233
4-lifters mill	80	yes	yes	no	9.05	165.68	292.66	44.34	250	6	72	233
8-lifters mill	80	yes	yes	no	6.55	176.05	294.89	64.93	253	10	75	228
16-lifters mill	80	yes	yes	no	7.34	225.00	292.66	77.65	252	30	72	222
32-lifters mill	80	yes	yes	no	4.46	261.47	294.19	92.71	256	48	74	220

At first glance, the results of Figure 5 and Table 5 may seem simple software outputs from DEM. However, after simulations, all the required information is available on the motion of all individual particles so that the researcher (computer user) can examine the position of each individual particle and its motion, which leads to the identification of charge shoulder and toe points, which was the main purpose of this study.

Figure 6(a) shows the effect of the number of lifters on the charge head height when the mill rotates at 70% of its critical speed. As it can be seen, the addition of one lifter has no effect on increasing the height of the charge head. Adding 2, 4, and 8 lifters to the mill has a noticeable increase in charge height but adding 16 and 32 lifters to the mill increases the charge head significantly more. Figure 6(b) demonstrates the effect of the number of lifters on the impact zone length when the mill rotates at 70% of its critical speed. As it can be observed, in all cases, the addition of lifters has increased the impact zone length so there is a direct relationship between them. Adding 16 and 32 lifters to the mill has a significant effect on increasing the length of the impact zone, and thereby, improving the impact mechanism and performance of the mill. Figure 6(c) illustrates the effect of the number of lifters on the charge head height when the mill rotates at 80% of its critical speed. As it can be seen, all the lifters have a favorable effect on the head height. It can be concluded that at 80% of the critical speed, there is no need to add the number of lifters, and only one lifter can create the proper head. Figure 6(d) demonstrates the effect of the number of lifters on the impact zone length when the mill rotates at 80% of its critical speed. As it can be seen, similar to the 70% case, again increasing the number of lifters has increased the impact zone length in all cases so there is a direct relationship between them. As before, adding 16 and 32 lifters has the most positive effect on increasing the length of the impact zone, and thereby, enhancing the impact mechanism and improving the mill performance.

Figure 7(a) demonstrates the effect of increasing the mill speed on the charge head height. As it can be seen, in all cases, increasing the mill rotational speed to 80% has increased the charge head height resulting in increased impact mechanism and improved the mill performance. Also increasing the mill speed has the most positive effect on the 1-, 2-, 4-, and 8-lifter modes. Figure 7(b) demonstrates the effect of increasing the mill speed on the impact zone length. As it can be seen, in all cases, the increase in the critical speed has increased the length of the impact zone. However, its effect on the 8-, 16-, and 32-liter modes has been far more impressive. Therefore, a 8-lifter mill is recommended as the optimum mill in this study work because it increases both the head height and impact zone length at the lowest possible cost (fewer lifters).

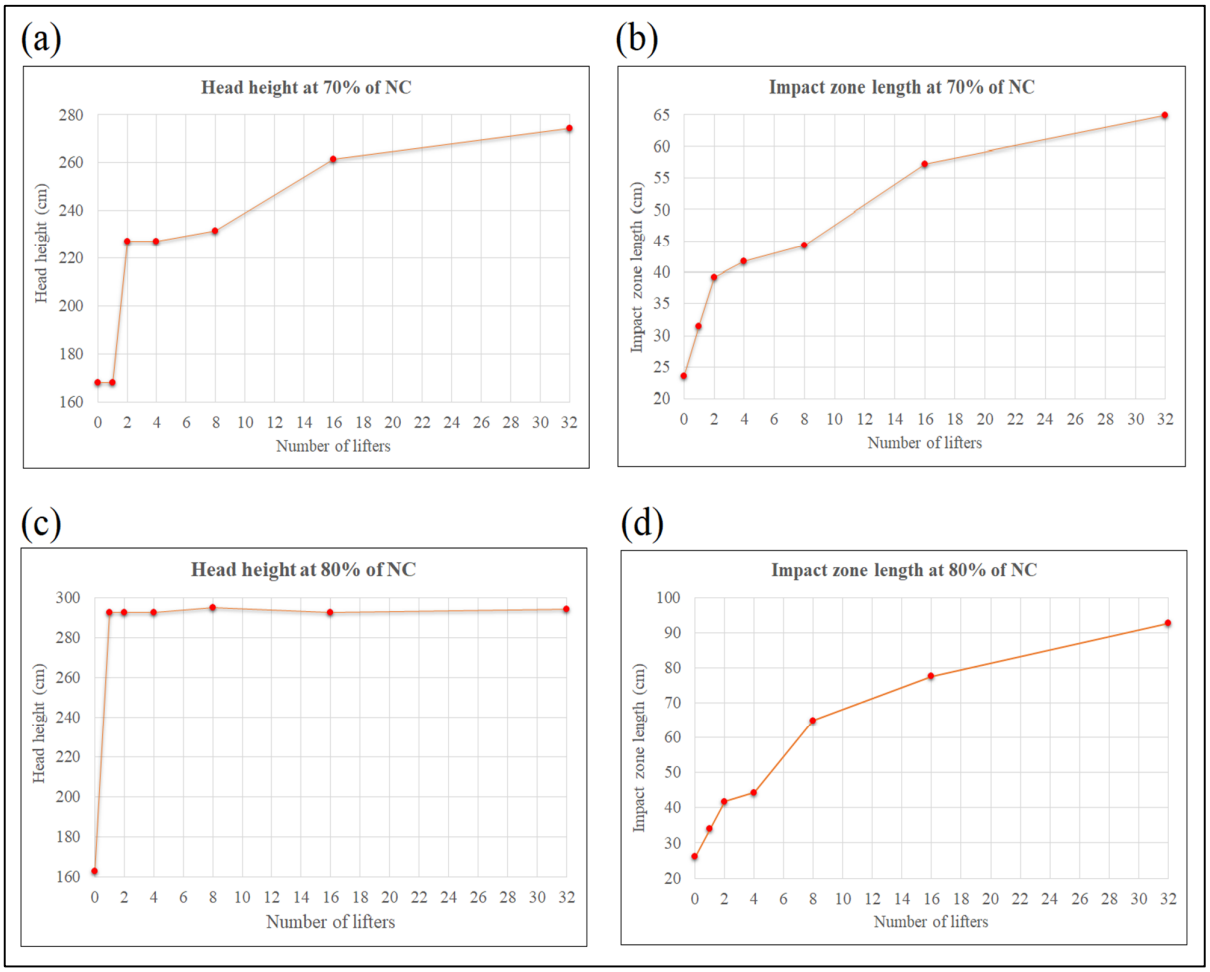

Figure 6. Effect of the number of lifters on charge (a) head height at 70% of N_C; (b) impact zone length at 70% of N_C; (c) head height at 80% of N_C; (d) impact zone length at 80% of N_C.

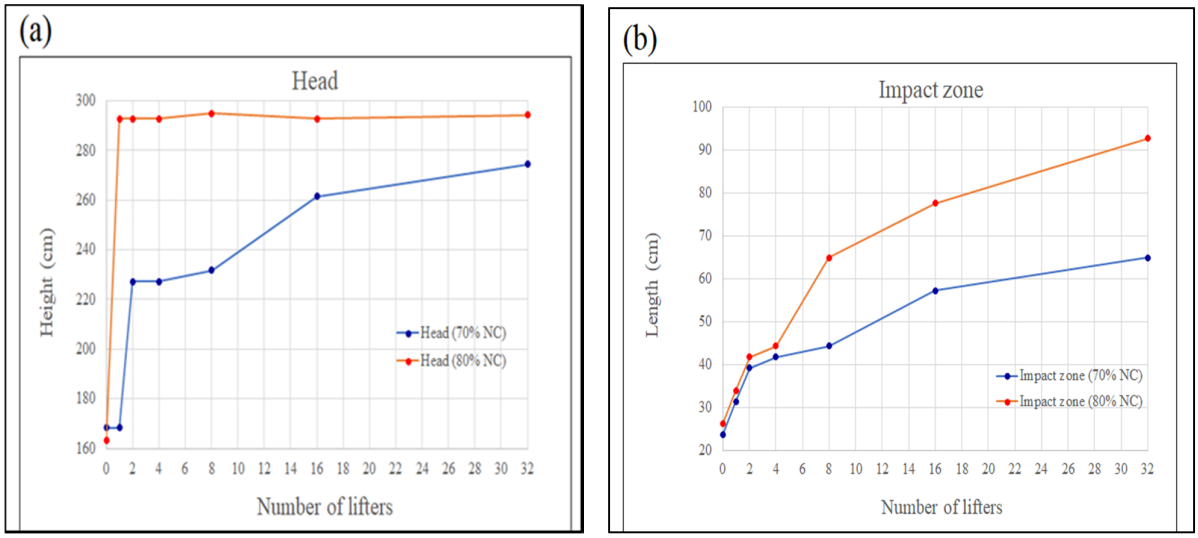

Figure 7. Effect of mill rotation speed on charge (a) head height; (b) impact zone length.

Figure 8 examines the impact of mill speed on the charge head height and impact zone length simultaneously. As it can be seen, increasing the mill speed to 80% of its critical speed in the no-lifter mode has no effect on increasing the charge head and the impact zone length. In 1-, 2-, and 4-

lifter mills, increasing the mill speed has a significant effect on increasing the charge head height but has no effect on increasing the impact zone length. However, at 8-, 16-, and 32-lifter mills, increasing the mill speed increases both the head height and impact zone length, and thereby, increases the impact mechanism and improves the mill performance. In general, the eight-lifter mill that rotates at 80% of critical speed can be identified as the optimum mill in this study.

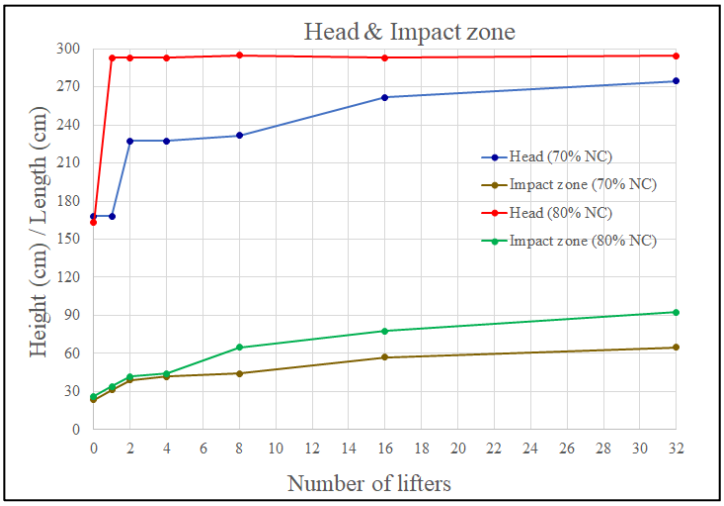

Figure 8. Effect of mill rotation speed on charge head heights and impact zone lengths.

4.1. Validation

Since the DEM approach offers such strong advantages in modeling and understanding the milling process, it is essential that both DEM simulations and the DEM solver are validated properly and adequately. In general, a comprehensive validation of the DEM solver and simulations is not feasible and, in most cases, it can be done only partially. In order to ensure the integrity of the application of the DEM techniques to comminution technology and other possible areas, the quality of validation should be improved and directed at the outputs being used in the modeling [51].

In this work, in order to validate the simulation results, a laboratory-scale SAG mill is simulated (Figure 9). The laboratory-scale SAG mill is according to the dimensions described in Bian et al. [24]. The detailed geometrical and operational conditions and material properties for the laboratory-scale SAG mill are listed in Tables 6–8, respectively.

In order to validate the obtained results and also the LIGGGHTS DEM solver, the charge head height and impact zone length of simulations conducted by this software for the laboratory-scale SAG mill are compared with the charge head height and impact zone length of experimental results under the similar conditions (Figures. 10–12 and Table 9). The high agreement between the results indicates their validity and also the validity of the DEM solver.

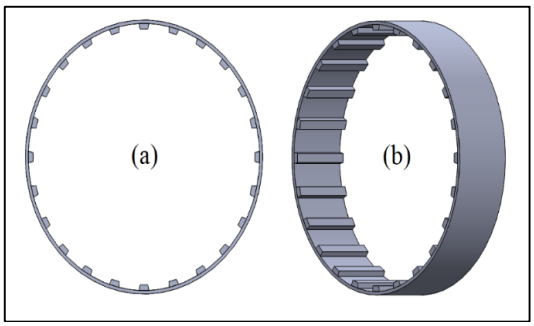

Figure 9. Laboratory-scale SAG mill (a) 2D geometry; (b) 3D geometry.

Table 6. Laboratory-scale SAG mill dimensions and speeds [24].

Laboratory-scale SAG mill	Dimensions
Shell thickness (cm)	0.75
Mill length (cm)	16
Mill diameter (cm)	57.3
Mill volume (cm^3)	41259
N_C (critical speed) (rpm)	56.88
Rotation speed (60% of N_C) (rpm)	32.79
Rotation speed (70% of N_C) (rpm)	38.26
Rotation speed (75% of N_C) (rpm)	40.99
Rotation speed (80% of N_C) (rpm)	43.72
Rotation speed (90% of N_C) (rpm)	49.19
Direction of rotation of mill	Clockwise
Trapezoid lifter length (cm)	16
Trapezoid lifter thickness (cm)	1.20
Trapezoid lifter widths (cm)	1.95 and 2.45

Table 7. DEM ball size distribution and numbers [24].

Ball size class (mm)	Number of balls	Mass fraction (%)
20	111	5.68
15	795	17.16
13	3051	42.87
8	10474	34.29
Total	14331	100

Table 8. Parameters used for the DEM simulations of the laboratory-scale SAG mill [24].

DEM model details	Value
% Fill of ball charge	40
Total mass of ball charge (kg)	62.8734
DEM spring constant (kg/m)	10^6
Ball density (kg/m^3)	7800
Ball sliding friction coefficient	0.5
Ball rolling friction coefficient	0.01
Poisons ratio	0.25
Young's modulus (N/m^2)	1×10^9
Ball restitution coefficient	0.5

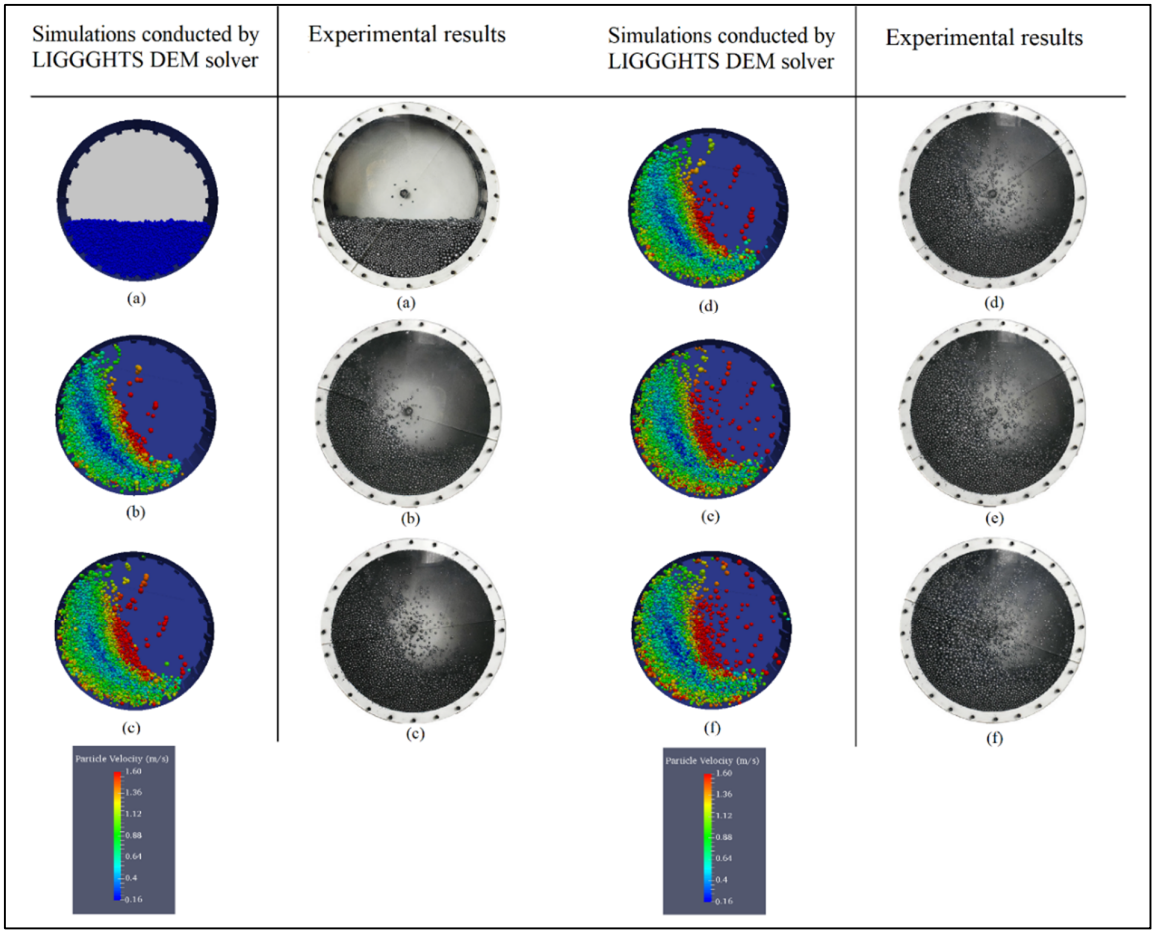

Figure 10. Comparison between simulations of the laboratory-scale SAG mill using LIGGGHTS DEM solver and experimental results [24] at the same operating conditions when the drum is rotating at (a) 0% of N_C; (b) 60% of N_C; (c) 70% of N_C; (d) 75% of N_C; (e) 80% of N_C; and (f) 90% of N_C.

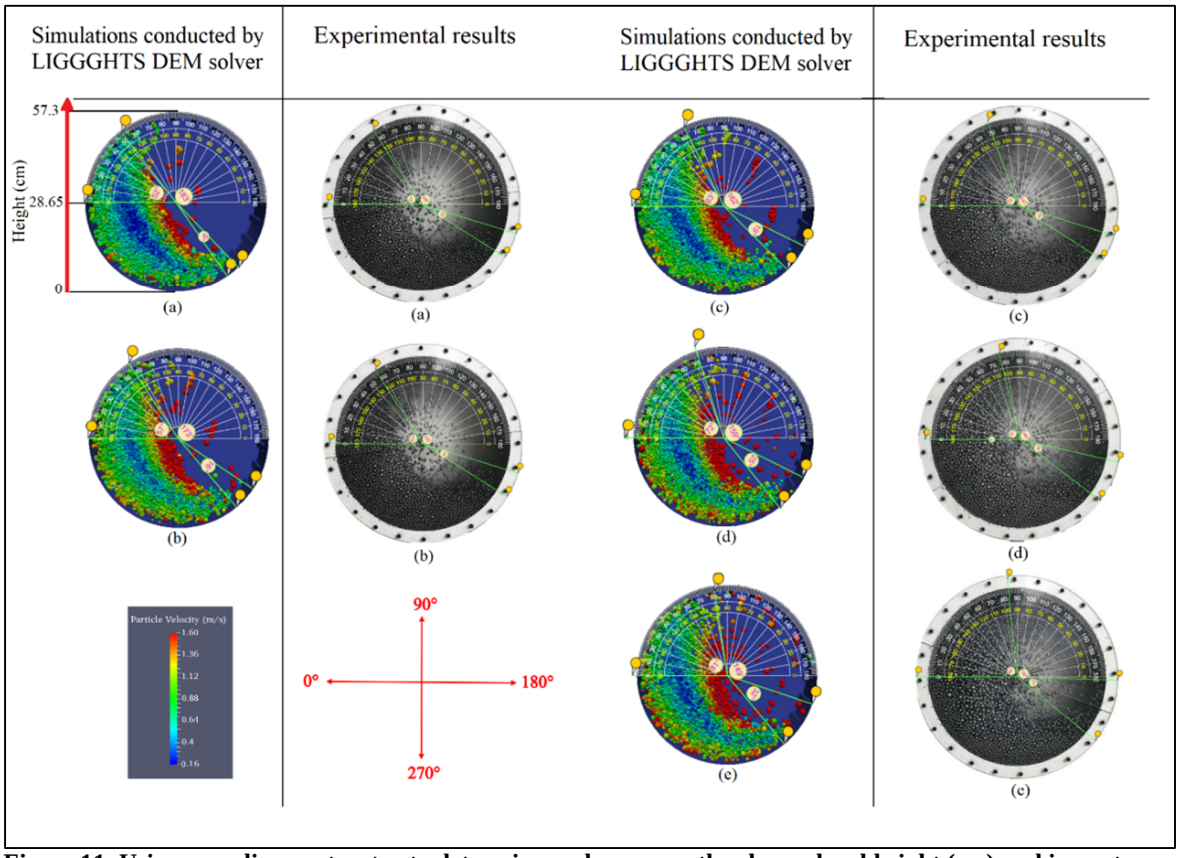

Figure 11. Using an online protractor to determine and compare the charge head height (cm) and impact zone length (cm) of simulations of the laboratory-scale SAG mill using LIGGGHTS DEM solver and real pictures of experimental results at the same operating conditions when the drum is rotating at (a) 0% of N_C; (b) 60% of N_C; (c) 70% of N_C; (d) 75% of N_C; (e) 80% of N_C; and (f) 90% of N_C.

Table 9. Comparison of the charge head height (cm) and impact zone length (cm) of simulations of the laboratory-scale SAG mill using LIGGGHTS DEM solver and real pictures of experimental results [24] at the same operating conditions.

Simulations of the laboratory-scale SAG mill				Real pictures of experimental results			
Mill rotation speed (rpm)	Mill rotation speed (%)	Head height (cm)	Impact zone length (cm)	Mill rotation speed (rpm)	Mill rotation speed (%)	Head height (cm)	Impact zone length (cm)
32.79	60% of N_C	51.23	4.50	32.79	60% of N_C	50.92	4.99
38.26	70% of N_C	52.68	7.97	38.26	70% of N_C	52.68	7.48
40.99	75% of N_C	54.18	9.46	40.99	75% of N_C	55.57	7.97
43.72	80% of N_C	55.90	12.40	43.72	80% of N_C	56.57	11.91
49.19	90% of N_C	56.95	15.79	49.19	90% of N_C	57.14	18.18

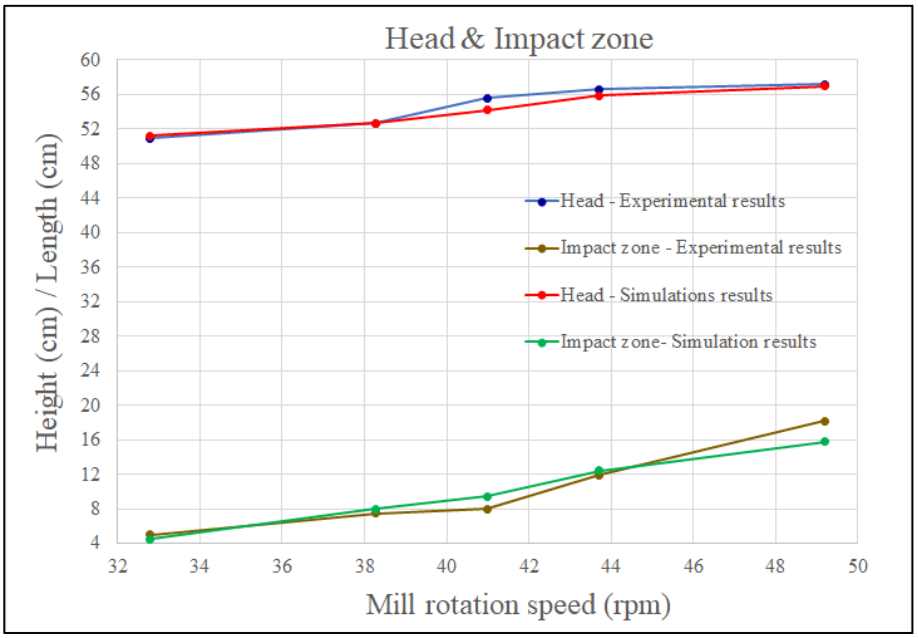

Figure 12. Validation of simulation results of the laboratory-scale SAG mill by comparison with experimental results at the same operating conditions at different mill rotation speeds (rpm).

5. Conclusions

In this research, an open-source software, LIGGGHTS, was used to perform DEM simulations of pilot-scale SAG mills. Also for the first time, the effect of the number of lifters of mill shell liners on two new parameters introduced by the authors, i.e. 'head height' and 'impact zone length', were investigated. The main innovation and novelty of the paper were introducing and basing these two parameters to evaluate and determine the trajectory of ball motion for investigating impact mechanism and improving performance of pilot-scale SAG mills.

The following results were obtained:

- Charge shoulder and charge toe heights were not suitable criteria for evaluating mill performance and impact mechanism. In this paper, the head height and impact zone length were replaced as appropriate criteria.
- In all simulations, a cascade motion was observed.
- For 70% of critical speed, no cataract motion was observed in no-lifter and one-lifter modes. However, it was observed for other modes.
- At 80% of critical speed, there was no cataract motion only for the no-lifter mode but there was for the other modes.
- In general, when the mill rotated at both 70% and 80% of its critical speed, head height and impact zone length increased as the number of lifters increased.
- In all cases, the addition of lifters increased the impact zone length, so there was a direct relationship between them.
- At 80% of the critical speed, there was no need to add the number of lifters and only one lifter could create the proper head.
- Generally, an increase of mill speed to 80% of its critical speed in all cases increased the charge head height and impact zone length.
- Increasing the mill speed to 80% of its critical speed in the no-lifter mode had no effect on increasing the charge head and impact zone length. In 1-, 2-, and 4-lifter mills, increasing the mill speed had a significant effect on increasing the charge head height but had no effect on increasing the impact zone length. However, at 8-, 16-, and 32-lifter mills, increasing the mill speed increased both the head height and the impact zone length, and thereby, increasing the impact mechanism and improving the mill performance.
- In general, the eight-lifter mill that rotated at 80% of critical speed could be identified as the optimum mill in this study because it increased both the head height and the impact zone length at the lowest possible cost (fewer lifters).
- Increasing the mill speed to 80% of its critical speed had a decreasing effect on the charge head height increase. However, it had

an increasing effect on the process of increasing the impact zone length.

- In order to validate the simulation results, a laboratory-scale SAG mill was simulated. Comparison of the simulations related to the laboratory-scale SAG mill with the experimental results demonstrated a good agreement, which validated the DEM simulations and the software used.
- Finally, the results obtained indicated that the charge heads were, respectively, raised about 106.08, 93.19, 63.42, 58.98, 58.98, and 0.00 cm at the simulations performed with 32, 16, 8, 4, 2, and 1 rectangle lifter(s), respectively, in comparison with the no-lifter case at 70% of N_C. The corresponding values at 80% of N_C were as follow: 131.12, 129.59, 131.82, 129.59, 129.59, and 129.59 cm.
- On the other hand, the impact zone lengths also were, respectively, increased about 41.39, 33.70, 20.81, 18.21, 15.62, and 7.82 cm at the simulations performed with above-mentioned lifters in comparison to the no-lifter case at 70% of N_C. The corresponding values for the impact zone lengths at 70% of its critical speed were as follow: 66.56, 51.50, 38.79, 18.20, 15.61, and 7.81 cm.
- Generally, the results obtained indicated that the optimum number of lifters for pilot-scale SAG mills was between 16 and 32 lifters with medium thickness. Liners with the number of lifters in this range required less mill speed to create cataract motions. However, liners with the number of lifters less than this range required a higher mill speed. Also liners with a number of lifters beyond this range required less mill speed, and they could cause centrifugal motions in the balls.

Acknowledgments

The authors wish to thank the Shahrood University of Technology and Professor Mohammad Ataei for providing the supercomputer required for DEM simulations.

References

[1]. Rosales-Marín, G., Andrade, J., Alvarado, G., Delgadillo, J.A. and Tuzcu, E.T. (2019). Study of lifter wear and breakage rates for different lifter geometries in tumbling mill: Experimental and simulation analysis using population balance model. Minerals Engineering. 141: 105857.

[2]. Mishra, B.K. and Rajamani, R.K. (1992). The discrete element method for the simulation of ball mills. Applied Mathematical Modelling. 16 (11): 598-604.

[3]. Powell, M.S. and McBride, A.T. (2004). A three-dimensional analysis of media motion and grinding regions in mills. Minerals Engineering. 17 (11-12): 1099-1109.

[4]. Cleary, P.W. (1998). Predicting charge motion, power draw, segregation and wear in ball mills using discrete element methods. Minerals Engineering. 11 (11): 1061-1080.

[5]. Cleary, P.W. (2001). Charge behaviour and power consumption in ball mills: sensitivity to mill operating conditions, liner geometry and charge composition. International journal of mineral processing. 63 (2): 79-114.

[6]. Kalala, J.T., Bwalya, M. and Moys, M.H. (2005). Discrete element method (DEM) modelling of evolving mill liner profiles due to wear. Part II. Industrial case study. Minerals Engineering. 18 (15): 1392-1397.

[7]. Kalala, J.T., Bwalya, M. and Moys, M.H. (2005). Discrete element method (DEM) modelling of evolving mill liner profiles due to wear. Part II. Industrial case study. Minerals Engineering. 18 (15): 1392-1397.

[8]. Banisi, S. and Hadizadeh, M. (2007). 3-D liner wear profile measurement and analysis in industrial SAG mills. Minerals Engineering. 20 (2): 132-139.

[9]. Yahyaei, M., Banisi, S. and Hadizadeh, M. (2009). Modification of SAG mill liner shape based on 3-D liner wear profile measurements. International Journal of Mineral Processing. 91 (3-4): 111-115.

[10]. Cleary, P.W. (2001). Recent advances in DEM modelling of tumbling mills. Minerals Engineering. 14 (10): 1295-1319.

[11]. El-Rahman, M.A., Mishra, B.K. and Rajamani, R.K. (2001). Industrial tumbling mill power prediction using the discrete element method. Minerals engineering. 14 (10): 1321-1328.

[12]. Cleary, P.W., Morrisson, R. and Morrell, S. (2003). Comparison of DEM and experiment for a scale model SAG mill. International Journal of Mineral Processing. 68 (1-4): 129-165.

[13]. Mishra, B.K. (2003). A review of computer simulation of tumbling mills by the discrete element method: part I—contact mechanics. International journal of mineral processing. 71 (1-4): 73-93.

[14]. Morrison, R.D. and Cleary, P.W. (2004). Using DEM to model ore breakage within a pilot scale SAG mill. Minerals Engineering. 17 (11-12): 1117-1124.

[15]. Djordjevic, N., Shi, F.N. and Morrison, R. (2004). Determination of lifter design, speed and filling effects in AG mills by 3D DEM. Minerals Engineering. 17 (11-12): 1135-1142.

[16]. Djordjevic, N., Morrison, R., Loveday, B. and Cleary, P. (2006). Modelling comminution patterns within a pilot scale AG/SAG mill. Minerals Engineering. 19 (15): 1505-1516.

[17]. Maleki-Moghaddam, M., Ghasemi, A.R., Yahyaei, M. and Banisi, S. (2015). The impact of end-wall effect on the charge trajectory in tumbling model mills. International Journal of Mineral Processing. 144: 75-80.

[18]. Owen, P. and Cleary, P.W. (2015). The relationship between charge shape characteristics and fill level and lifter height for a SAG mill. Minerals Engineering. 83: 19-32.

[19]. Weerasekara, N.S., Liu, L.X. and Powell, M.S. (2016). Estimating energy in grinding using DEM modelling. Minerals Engineering. 85: 23-33.

[20]. Cleary, P.W. and Owen, P. (2018). Development of models relating charge shape and power draw to SAG mill operating parameters and their use in devising mill operating strategies to account for liner wear. Minerals Engineering. 117: 42-62.

[21]. Xu, L., Luo, K. and Zhao, Y. (2018). Numerical prediction of wear in SAG mills based on DEM simulations. Powder Technology, 329, 353-363.

[22]. Cleary, P.W. and Owen, P. (2019). Effect of operating condition changes on the collisional environment in a SAG mill. Minerals Engineering. 132: 297-315.

[23]. Hasankhoei, A.R., Maleki-Moghaddam, M., Haji-Zadeh, A., Barzgar, M.E. and Banisi, S. (2019). On dry SAG mills end liners: Physical modeling, DEM-based characterization and industrial outcomes of a new design. Minerals Engineering. 141: 105835.

[24]. Bian, X., Wang, G., Wang, H., Wang, S. and Lv, W. (2017). Effect of lifters and mill speed on particle behaviour, torque, and power consumption of a tumbling ball mill: Experimental study and DEM simulation. Minerals Engineering. 105: 22-35.

[25]. Pedrayes, F., Norniella, J.G., Melero, M.G., Menéndez-Aguado, J.M. and del Coz-Diaz, J.J. (2018). Frequency domain characterization of torque in tumbling ball mills using DEM modelling: Application to filling level monitoring. Powder Technology, 323, 433-444.

[26]. Chegeni, M.J. and Kolahi, S. An investigation on effect of shell liner type on performance of industrial SAG mills using DEM.

[27]. Cleary, P.W. (2004). Large scale industrial DEM modelling. Engineering Computations.

[28]. Cleary, P.W., Sinnott, M.D. and Morrison, R.D. (2008). DEM prediction of particle flows in grinding processes. International Journal for numerical methods in fluids. 58 (3): 319-353.

[29]. Cleary, P.W. (2009). Ball motion, axial segregation and power consumption in a full scale two chamber cement mill. Minerals Engineering. 22 (9-10): 809-820.

[30]. Kozicki, J. and Donze, F.V. (2009). YADE-OPEN DEM: An open-source software using a discrete element method to simulate granular material. Engineering Computations.

[31]. Chen, J., Huang, B., Chen, F. and Shu, X. (2012). Application of discrete element method to Superpave gyratory compaction. Road materials and pavement design. 13 (3): 480-500.

[32]. Zhang, L., Quigley, S.F. and Chan, A.H. (2013). A fast scalable implementation of the two-dimensional triangular Discrete Element Method on a GPU platform. Advances in Engineering Software. 60: 70-80.

[33]. Kruggel-Emden, H., Sturm, M., Wirtz, S. and Scherer, V. (2008). Selection of an appropriate time integration scheme for the discrete element method (DEM). Computers & Chemical Engineering. 32 (10): 2263-2279.

[34]. Nassauer, B., Liedke, T. and Kuna, M. (2013). Polyhedral particles for the discrete element method. Granular matter. 15 (1): 85-93.

[35]. Raji, A.O. and Favier, J.F. (2004). Model for the deformation in agricultural and food particulate materials under bulk compressive loading using discrete element method. I: Theory, model development and validation. Journal of food engineering. 64 (3): 359-371.

[36]. Nassauer, B. and Kuna, M. (2013). Contact forces of polyhedral particles in discrete element method. Granular Matter. 15 (3): 349-355.

[37]. Balevičius, R., Džiugys, A., Kačianauskas, R., Maknickas, A. and Vislavičius, K. (2006). Investigation of performance of programming approaches and languages used for numerical simulation of granular material by the discrete element method. Computer Physics Communications. 175 (6): 404-415.

[38]. Delaney, G.W., Cleary, P.W., Morrison, R.D., Cummins, S. and Loveday, B. (2013). Predicting breakage and the evolution of rock size and shape distributions in Ag and SAG mills using DEM. Minerals Engineering. 50: 132-139.

[39]. Ting, J.M., Khwaja, M., Meachum, L.R. and Rowell, J.D. (1993). An ellipse-based discrete element model for granular materials. International Journal for Numerical and Analytical Methods in Geomechanics. 17 (9): 603-623.

[40]. Shmulevich, I. (2010). State of the art modeling of soil–tillage interaction using discrete element method. Soil and Tillage Research. 111 (1): 41-53.

[41]. Cleary, P.W. and Sawley, M.L. (2002). DEM modelling of industrial granular flows: 3D case studies and the effect of particle shape on hopper discharge. Applied Mathematical Modelling. 26 (2): 89-111.

[42]. Munjiza, A. and Cleary, P.W. (2009). Industrial particle flow modelling using discrete element method. Engineering Computations.

[43]. Cleary, P.W. and Sinnott, M.D. (2008). Assessing mixing characteristics of particle-mixing and granulation devices. Particuology. 6 (6): 419-444.

[44]. Cleary, P.W. (2010). DEM prediction of industrial and geophysical particle flows. Particuology. 8 (2): 106-118.

[45]. Cleary, P.W. and Morrison, R.D. (2009). Particle methods for modelling in mineral processing. International Journal of Computational Fluid Dynamics. 23 (2): 137-146.

[46]. Just, S., Toschkoff, G., Funke, A., Djuric, D., Scharrer, G., Khinast, J. and Kleinebudde, P. (2013). Experimental analysis of tablet properties for discrete element modeling of an active coating process. AAPS PharmSciTech. 14 (1): 402-411.

[47]. McBride, W. and Cleary, P.W. (2009). An investigation and optimization of the 'OLDS'elevator using Discrete Element Modeling. Powder Technology. 193 (3): 216-234.

[48]. Goniva, C., Kloss, C., Deen, N.G., Kuipers, J.A. and Pirker, S. (2012). Influence of rolling friction on single spout fluidized bed simulation. Particuology. 10 (5): 582-591.

[49]. Goniva, C., Kloss, C., Hager, A. and Pirker, S. (2010, June). An open source CFD-DEM perspective. In Proceedings of OpenFOAM Workshop, Göteborg (pp. 22-24).

[50]. Kloss, C., Goniva, C., Aichinger, G. and Pirker, S. (2009). Comprehensive DEM-DPM-CFD simulations-model synthesis, experimental validation and scalability. In Proceedings of the seventh international conference on CFD in the minerals and process industries, CSIRO, Melbourne, Australia.

[51]. Weerasekara, N.S., Powell, M.S., Cleary, P.W., Tavares, L.M., Evertsson, M., Morrison, R.D. and Carvalho, R.M. (2013). The contribution of DEM to the science of comminution. Powder Technology, 248, 3-24.

بررسی تأثیر تعداد لیفترها بر عملکرد آسیاهای نیمه‌خودشکن مقیاس پایلوت با استفاده از روش اجزای گسسته

سجاد کلاهی و محمد جهانی چگنی*

دانشکده مهندسی معدن، نفت و ژئوفیزیک، دانشگاه صنعتی شاهرود، ایران

ارسال 2019/10/21، پذیرش 2020/2/24

* نویسنده مسئول مکاتبات: M.Jahani@shahroodut.ac.ir

چکیده:

تعداد لیفترهای لاینرهای پوسته آسیا، سرعت چرخش آسیا، و درصد پرشدگی بار خردکننده سه تا از مهمترین پارامترهایی هستند که رفتار بار و مسیر حرکت گلوله‌ها درون آسیاهای نیمه‌خودشکن و در نتیجه عملکرد آن‌ها را تحت تأثیر قرار می‌دهند. در این مقاله، عملیات آسیاکنی آسیاهای نیمه‌خودشکن مقیاس پایلوت با استفاده از روش اجزای گسسته (راگ) بررسی شده است. در ابتدا، یک آسیای نیمه‌خودشکن مقیاس پایلوت با ابعاد 3/0 متر در 1/5 متر بدون هیچ لیفتری شبیه‌سازی شده است. سپس با افزودن به ترتیب یک، دو، چهار، هشت، شانزده، و سی و دو لیفتر(های) مستطیلی، شش شبیه‌سازی مستقل دیگر انجام شدند. تأثیرات تعداد لیفترها بر دو پارامتر جدید معرفی‌شده بوسیله مؤلفان یعنی «ارتفاع هد» و «طول زون ضربه» و نیز بر ایجاد حرکات آبشاری کوچک، آبشاری بزرگ، و گریز از مرکز برای گلوله‌ها در دو سرعت متفاوت آسیا، یعنی 70 درصد و 80 درصد سرعت بحرانی آن (N_C) مورد ارزیابی قرار گرفتند. همچنین به منظور اعتبارسنجی کردن نتایج شبیه‌سازی‌ها، یک آسیای نیمه‌خودشکن مقیاس آزمایشگاهی شبیه‌سازی شده است. نتایج حاصل نشان دادند که تعداد بهینه لیفترها برای آسیاهای نیمه‌خودشکن مقیاس پایلوت بین 16 تا 32 لیفتر با ضخامت متوسط است. لاینرهای با تعداد لیفترها در این محدوده به سرعت کمتر آسیا برای ایجاد حرکات آبشاری بزرگ نیاز دارند. اما لاینرهای با تعداد لیفترهای کمتر از این محدوده به یک سرعت آسیای بالاتر نیاز دارند. همچنین، لاینرهای با تعداد لیفترها فراتر از این محدوده به سرعت کمتر آسیا نیاز دارند و می توانند حرکات گریز از مرکز در گلوله‌ها ایجاد کنند. مقایسه شبیه‌سازی‌های مربوط به آسیای نیمه‌خودشکن مقیاس آزمایشگاهی با نتایج تجربی تطابق خوبی را نشان می‌دهد، که شبیه‌سازی‌های راگ و نرم‌افزار استفاده‌شده را اعتبارسنجی می‌کند.

کلمات کلیدی: شبیه‌سازی راگ، آسیای نیمه‌خودشکن مقیاس پایلوت، تعداد لیفترها، ارتفاع هد، طول زون ضربه.